



Assessment of Ground Penetrating Radar for Pyrite Swelling Detection in Soils

Nabil KhoderAgha ^{1*}, Gabriel Assaf ¹

¹ Faculty of Construction Engineering, École de Technologie Supérieure, 1100 Notre-Dame St. W, Montreal, QC H3C 1K3, Canada.

Received 26 October 2023; Revised 21 February 2024; Accepted 25 February 2024; Published 01 March 2024

Abstract

Pyrite swelling in soils below buildings is a major issue. It leads to severe deformations in floor foundations. A survey is carried out at a selected site in the city of Laval, Quebec, to assess the usefulness of ground-penetrating radar (GPR) to detect deformations that may be indicative of the presence of pyrite. Four soil samples are taken from the aforementioned site to determine the soil type below the concrete slab. The results indicate the presence of limestone, moor clay, and shale sediments, which are prone to pyrite swelling. The GPR data were collected using the GSSI SIR 4000 with a high frequency antenna and processed using RADAN software. The GPR data indicate the presence of severe deformation in many locations of the concrete slab. The most important wave reflections indicative of pyrite swelling are the rebar reflections, showing interesting pushed-up and dropped-down reflections. These reflections appear in two forms. The first is the attenuated reflections that may occur due to pyrite-rich materials. The second is the high amplitude reflections that occur because of the air void, which can be formed due to heaving the concrete slab because of pyrite swelling. As a result, GPR appears to be an effective method for assessing and mapping the effect of pyrite swelling below concrete slabs.

Keywords: Assessment; Ground Penetrating Radar; Radan; Pyrite.

1. Introduction

Major issues with concrete slabs occur in buildings that are constructed on compact rock fills containing pyrite, particularly black shale and mudstone. Pyrite oxidizes when shale is excavated or used as a foundation material. Pyrite is very sensitive to humidity, whereas even a very small amount of water can lead to the Pyrite reaction [1]. Pyrite problems are observed as swelling shale bedrock affects the foundations and concrete slab on grade of buildings. The first documented case of pyrite swelling in bedrock was reported in Canada in the late 1960s [2]. Such swelling issues often take a considerable amount of time to become evident. For instance, it took approximately 20 years to diagnose that the swelling problems in Quebec City were caused by pyrite [3]. Similarly, numerous cases of concrete heaving due to pyrite swelling have been reported in the UK [4], Ireland [2], the USA [1], and Japan [5].

The effect of pyrite on building foundations is well discussed and documented in the literature. Hawkins and John report that oxygen and moisture are key factors that help pyrite crystallisation within most rock types, leading to swelling and thereby extensive damage to the concrete slab [6, 7]. This damage may be observed either in the concrete itself as result of pyrite presence in the aggregate within the mix or in the soil underneath the slab. Maher & Gray report that serious pyrite swelling problems in the concrete slabs that occurred in a large number of buildings in Ireland and Canada were due to the use of mudstone aggregation, which contains pyrite crystals [2]. Hoover et al. report severe cracks in concrete slabs in the Evangelical Hospital in Pennsylvania, USA, due to swelling of the underlying soil, which consists

* Corresponding author: nabil.khoderagha.1@ens.etsmtl.ca

 <http://dx.doi.org/10.28991/CEJ-2024-010-03-05>



© 2024 by the authors. Licensee C.E.J, Tehran, Iran. This article is an open access article distributed under the terms and conditions of the Creative Commons Attribution (CC-BY) license (<http://creativecommons.org/licenses/by/4.0/>).

of weathered shale fragments [8]. They suggested additional laboratory research to produce better identification tools for geotechnical engineers unfamiliar with pyrite's expansive nature. Maher et al. describe a large-scale laboratory study involving pyrite-swelling tests conducted over two years [9]. The results demonstrate that mudstone swelling continues at a rate of 0.6% of the fill thickness per year, leading to significant building damage. Mckeen et al. proposed a novel physical model that provides a valuable framework for predicting the time required to generate specific amounts of floor movement in residential dwellings [10].

GPR has been widely used for various applications, including archaeology, geology, engineering, and environmental studies [11–15]. It provides high-resolution two-dimensional (2D) and three-dimensional (3D) images of the subsurface [11]. Furthermore, it is an economical, fast, and effective method compared with the traditional methods [16, 17].

Ground-penetrating radar (GPR) is a non-invasive, non-destructive method that offers precise imaging capabilities. It helps researchers and surveyors accurately locate and determine the depth of buried objects. It depends on emitting electromagnetic (EM) waves through the ground by a transmitting antenna. These EM waves will propagate and intersect any geological interface between two different materials that occurs due to any difference in the physical and chemical properties. As a result, the propagation velocity of the EM waves will change, and part of these waves will reflect back to the surface [18]. As such, the receiving antenna will record wavelength, amplitude, and the two-way travel time as shown in Figure 1.

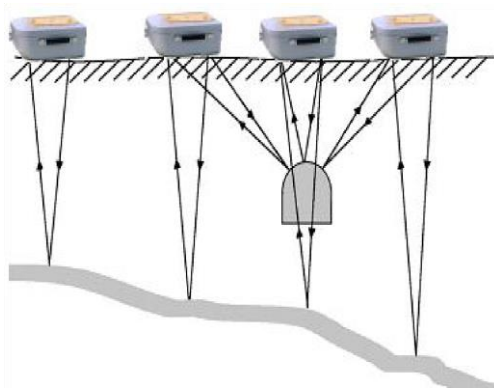


Figure 1. Illustrates the principle of ground penetrating radar detection

Many research studies discuss the effectiveness of the GPR to assess concrete slab conditions and to detect rebar, cracks, voids, and other issues in concrete. Oikonomopoulou et al. report a laboratory application of GPR on six concrete slabs, where several objects made of different materials are embedded within [19]. They concluded that the GPR is effective in the identification the embedded objects. They also found that the cross-polarization GPR antennas can detect different rebar diameters. Liu et al. propose a rebar detection method using deep learning and migration [20]. The results suggest that this method can automatically detect the rebar from the GPR image in real-time. Tian et al. detect and identify three major defects in concrete structures, including delamination, air void, and moisture by analyzing their reflection polarity [21]. Perez-Garcia et al. investigate cracks in concrete slab on grade with GPR [22]. Rahman M, et al. use a controlled laboratory environment to analyze the attenuation of GPR signals in concrete due to various subsurface defects and rebar [23]. The results show a variation in the measured reflected amplitudes for different materials due to differing dielectric constants. Dinh & Gucunski explore various factors that may affect the detectability of concrete delamination in GPR images [24]. They conclude that there is always a signal reflected whenever there is delamination or solid-air interface, with increasing signal strength with the thickness of the delamination. Rasol et al. reports a laboratory investigation to assess the ability of the GPR to detect and quantify cracks in concrete samples covered with asphalt [25]. The results showed that crack's width was detected in most cases with cross-polarisation.

No literature reports the use of GPR to detect the effect of pyrite swelling in concrete slabs. This paper reports research organized in two parts. The first part is to assess the soil composition beneath the slab to verify any evidence of pyrite existence in the soil. The second part is to delimitate the impacted pyrite swelling underneath the slab using a high-frequency GPR antenna, offering maximum resolution for targets within or just below the concrete slab.

2. Site Description and Fieldwork

The investigated site in a commercial building is located in the city of Laval, Canada, at latitude 45°33'12.96" N and Longitude 73°45'24.08" W, severe cracks and heaving are observed on concrete slabs on grade as presented in Figure 2. The fill materials beneath the concrete slab predominantly consist of clayey materials. Before collecting GPR data, Figure 3 shows that four soil samples were extracted directly from the area beneath the concrete slab. These samples were selected from the corners of the slab to identify and characterize the soil type underneath the slabs.

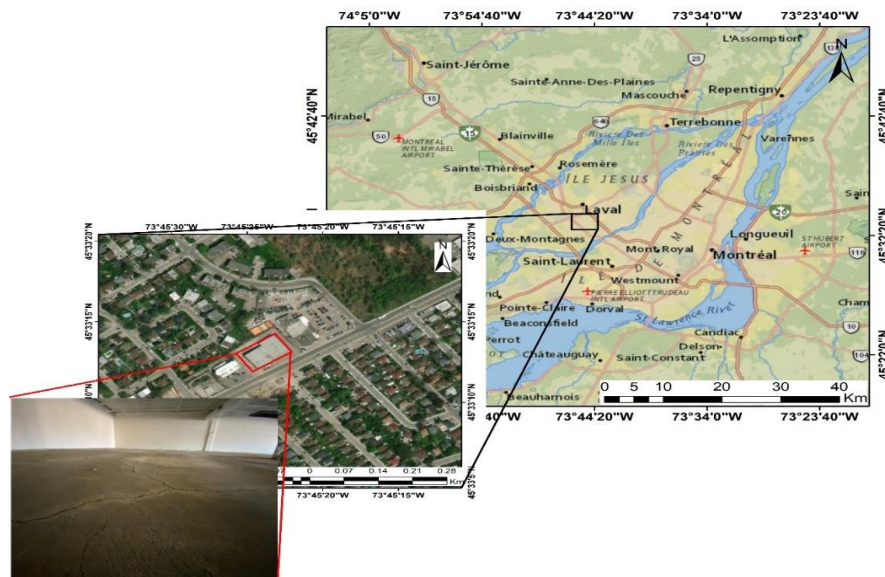


Figure 2. Location of the investigated site, the concrete slab is characterized by the presence of cracks and heaves that distributed along it

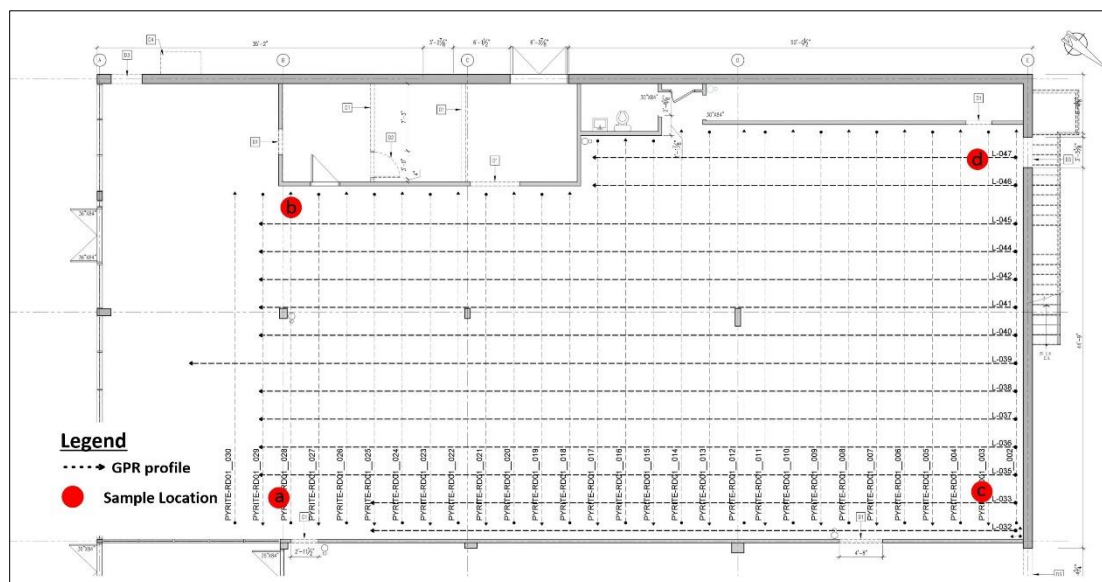


Figure 3. GPR profiles within the investigated site. Red dots represent the locations of the soil samples

The GPR data were collected using a Geophysical Survey Systems, Inc. (GSSI) SIR4000 pro console coupled with a 1600 MHz antenna [26]. The GPR data is collected within a grid measuring 14 x 28 m. This grid comprised 14 GPR profiles in the X-direction and 29 profiles in the Y-direction, with a 1-meter spacing between every two profiles as shown in Figure 3. The length of the profiles in the X-direction ranged between 23 m to 28 m, but most of the profiles were within 26 m long, while in the Y-direction, the profiles varied between 12 m and 14 m. The variation in profile lengths was adjusted by the presence of obstacles within the investigated site.

3. Data Processing and Interpretation

The processing and interpretation of the data are divided into two steps as shown in Figure 4. The first step is to identify and characterize the soil samples, while the second step collects, processes and interprets the GPR data.

The soil samples were analyzed using the CTQM200 protocol to determine the Petrographic Swelling Potential Index (PSPI) as tabulated in Table 1 [27]. This analysis involved testing of weighted soil groups extracted from various depths for each sample, Figure 3 presents the locations of the samples. Each weighted soil is treated to classify its components. Here, the components consist of twelve items and each item represents a soil type. However, only two main components respond to the PSPI. These components are Dolo Limestone/Clayey Dolomite and Shale. For each sample, the percentage of the practical fraction size (RF%) of the components was measured, and the PSPI was

subsequently calculated. The PSPI values are varied between 3.4 to 5.4 reflecting aggregates deemed to come from the right and left sides of the site. Consequently, the soil type can be classified as Ordovician limestone, more clayey in places, which probably intersects thin clayey beds and shale sediments. The Shale and clayey materials on the site are more likely to contain pyrite within their particles, which can react with air and moisture. Then pyrite swelling is probably the reason for the concrete slab deformation in the investigated site.

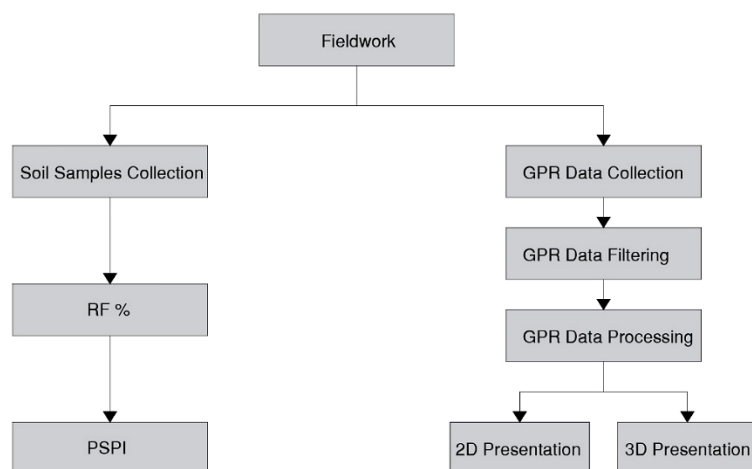


Figure 4. Flowchart of the research methodology

Table 1. PSPI test results

Sample (a)	Shale	Dolo limestone/ Clayey Dolomite
RF%*	2.10	13.0
PSPI Coefficient	1.00	0.10
PSPI**	2.10	1.30
PSPI (Shale+Dololimestone)***	3.4	
Sample (b)	Shale	Dololimestone/ Clayey Dolomite
RF%*	3.00	18.1
PSPI Coefficient	1.00	0.10
PSPI**	3.00	1.81
PSPI (Shale+Dololimestone)***	4.81	
Sample (c)	Shale	Dololimestone/ Clayey Dolomite
RF%*	3.40	20.0
PSPI Coefficient	1.00	0.10
PSPI**	3.40	2.00
PSPI (Shale+Dololimestone)***	5.40	
Sample (d)	Shale	Dololimestone/ Clayey Dolomite
RF%*	2.40	17.2
PSPI Coefficient	1.00	0.10
PSPI**	2.40	1.72
PSPI (Shale+Dololimestone)***	4.12	

* %RF = % compared to the % of the particle size fraction without debris;

** PSPI= Petrographic Swelling Potential Index;

*** PSPI Cumulative of the sample.

The GPR profiles were processed using RADAN software from the GSSI manufacturer. The processing involved several basic steps to enhance the quality of the 2D GPR profiles. These steps included time zero correction (0.703 ns), background removal, and Bandpass filter (500 MHz for high pass and 3000 MHz for low pass). These processing steps improve the clarity and accuracy of the GPR data. For the 3D GPR model, all the GPR profiles are migrated with a velocity of 0.09 m/ns and then the Hilbert transform is used as the final processing step. However, three main reflections are observed within the processed GPR profiles. These reflections correspond to the presence of rebar, voids, and utility lines presented Figure 5. These reflections provide valuable information about the subsurface conditions and can help in identifying potential areas of concern related to pyrite swelling and concrete slab deformation.

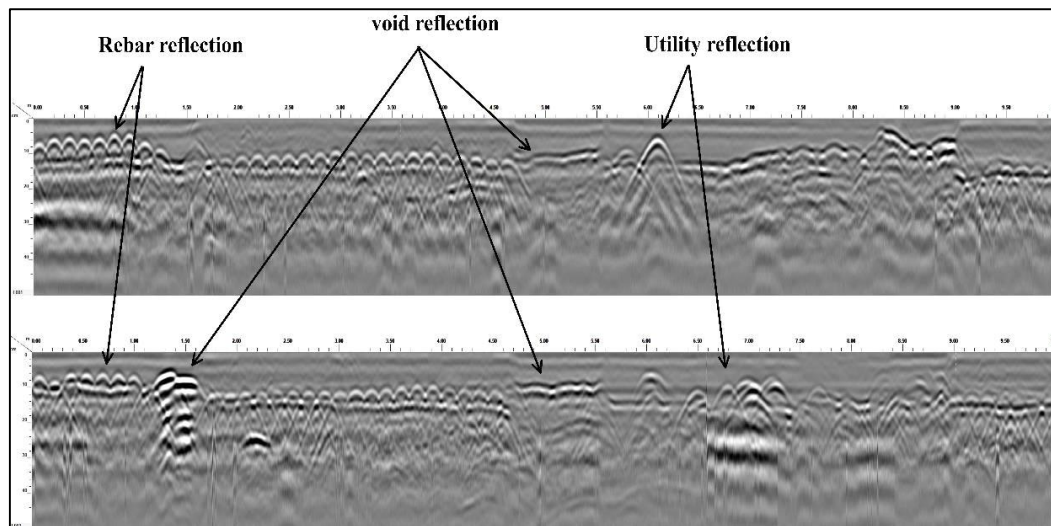


Figure 5. GPR profiles no. 10 and 12, showing rebar, void, and utility reflections

The rebar reflections in all the GPR profiles show clear deformation in their shapes and locations, indicating significant distortion of the concrete slab. This distortion is attributed to the swelling of the underlying soil that is caused by the reaction of pyrite with the surrounding materials shown in Figure 6. Normally, when the concrete slab is in good condition, the rebar mesh should appear at a consistent level. However, due to the severe impact of the swelling on the concrete slab, the rebar mesh is distorted. This deformation can therefore be considered as evidence of the presence of pyrite in the subsurface material.

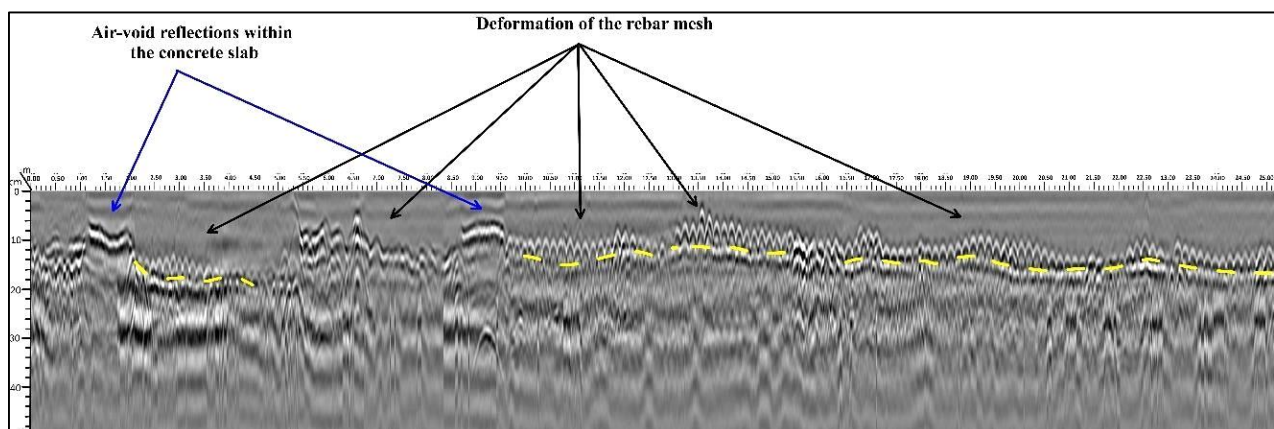


Figure 6. GPR profile no. 38, showing the rebar reflections are distorted due to the swelling, which severely effect the concrete slab

Figure 6 is a good example that shows the deformations in the slab where some parts of the rebar are slightly up and others are slightly down. The GPR profile no. 38 in Figure 6 shows that the thickness of the slab varies between 12 to 18 cm in depth. Furthermore, two distinctive reflections observed as a result of air voids inside or just beneath the concrete slab appear clearly in this profile. An interesting reflection is also shown in some GPR profiles, which indicates that part of the concrete slab is pushed up while the other parts remain at their locations, as shown in Figure 7. This reflection appears clearly at a depth of 8cm, while the other reflections appear at a depth of 16cm. This uplifted part of reflection may indicate two things. The first is an air void that is created just below the concrete slab. The second is that the reflections from the rebar are too weak. This phenomenon may occur for two reasons. The first reason is the high amplitude reflection of the air void, where the GPR waves speed up when traveling through the air void to reach airspeed, then severely slow down when hitting the underlying layer. Therefore, this high-amplitude reflection will cover the weaker reflections of the rebar. The second reason is the high attenuation that occurs due to the high conductivity of pyrite-rich materials [16] and their reaction with moisture [7]. It seems that the concentration of pyrite and moisture in this part of the slab is higher than in the other parts. Therefore, the reaction of pyrite with its surrounding materials may lead to attenuate the GPR wave and produce weak reflections. On the other hand, the other parts of reflection appear approximately at the same level as shown in Figure 7. This may indicate that this part of the concrete slab is intact, and mainly no pyrite swelling occurs at these parts.

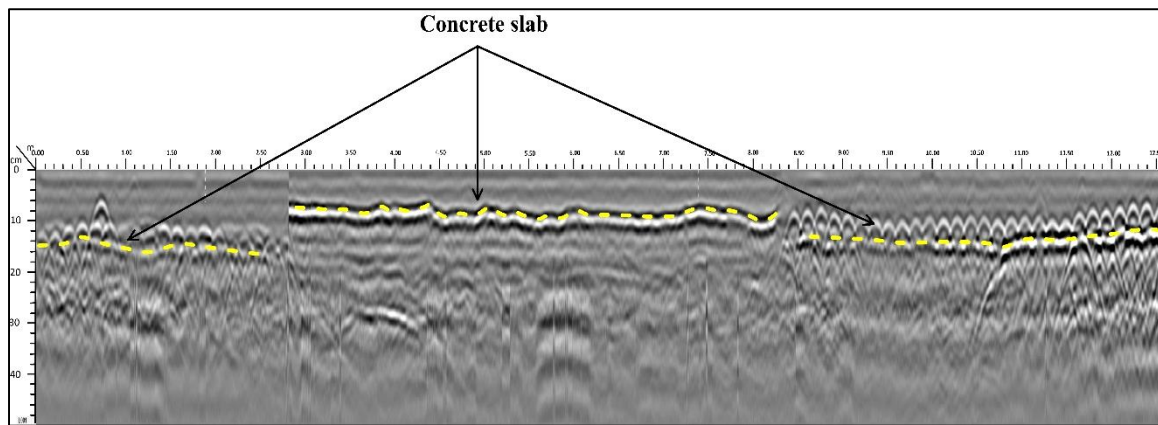


Figure 7. GPR profile no. 13, showing that the bottom of the concrete slab is pushed up due to swelling of underlying materials. The other parts of the slab remain at the same level

The 3D presentation shows how the high attenuation of the GPR waves, and the swelling of the underneath materials affect the GPR reflections. For instance, the cross-section of the GPR profiles No. 11 (in the Y-direction) and No. 45 (in the X-direction) reveals distinct zones of attenuation, as shown in Figure 8a. The effect of the swelling can also be seen along the cross-section, where some parts of the concrete slab are pushed up and others are dropped down. Additionally, multiple distinct reflections from air voids are observed on both GPR profiles at approximately the same level. These reflections collectively indicate that the deformation of the concrete slab is severe due to the reaction of pyrite with other materials. Another good example is shown in Figure 8b, where a cross-section of the GPR profiles No. 8 (in the Y-direction) and No. 37 (in the X-direction) is presented. Again, the zones of low and high amplitude reflections, as well as the upward and downward reflected parts, indicate the indirect impact of pyrite when it reacts with moisture and the surrounding materials. These sections effectively highlight the effect of pyrite swelling, which significantly attenuates the GPR reflections and leads to severe deformation in the concrete slab.

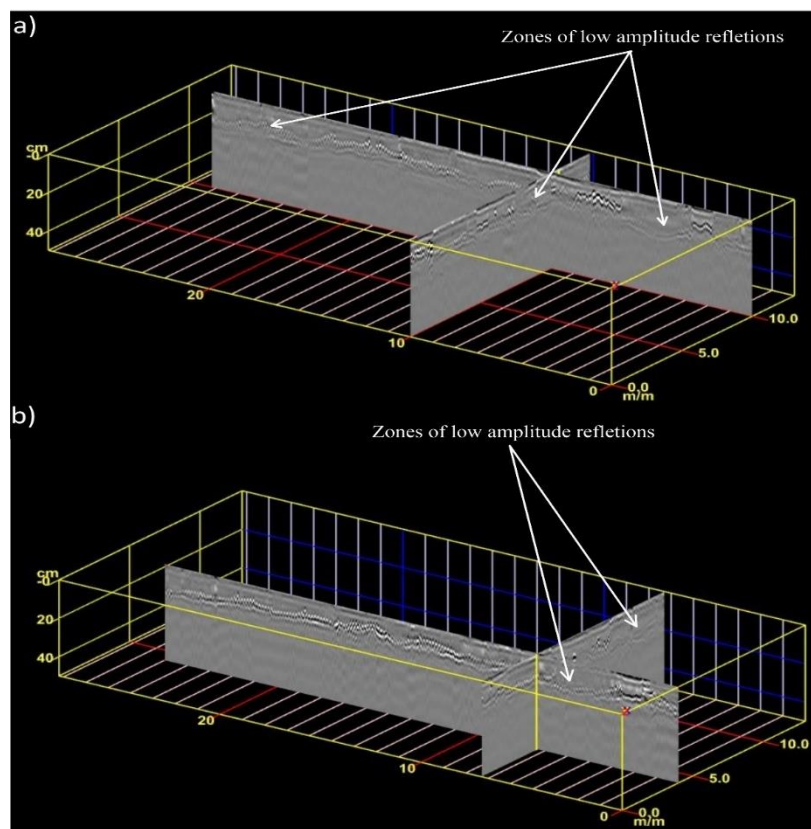


Figure 8. Low and high amplitude reflections zones

To obtain a more detailed understanding of the condition of the concrete slab and the underlying materials, a 3D Iso-surface map is derived from the grid of the GPR profiles at a depth of about 12 cm beneath the ground surface presented in Figure 9. Within this map, two significant areas are observed. The first area corresponds to the rebar mesh, which is visible in some locations. The amplitude strength of the rebar reflections on the map varies, ranging

from very high to low amplitude reflections. This variation is expected since the level of the rebar mesh is not uniform due to the swelling of the underlying soil. The second area looks vanished with no reflections. It seems that this area is the most affected by the attenuations and/or swelling of the underneath materials. This suggests that the concrete slab is severely affected in these regions of vanished reflections. However, this does not imply that the other rebar mesh areas are not affected by attenuation or swelling, but it seems that the concentration of pyrite in rebar mesh areas is relatively lower than in other areas.

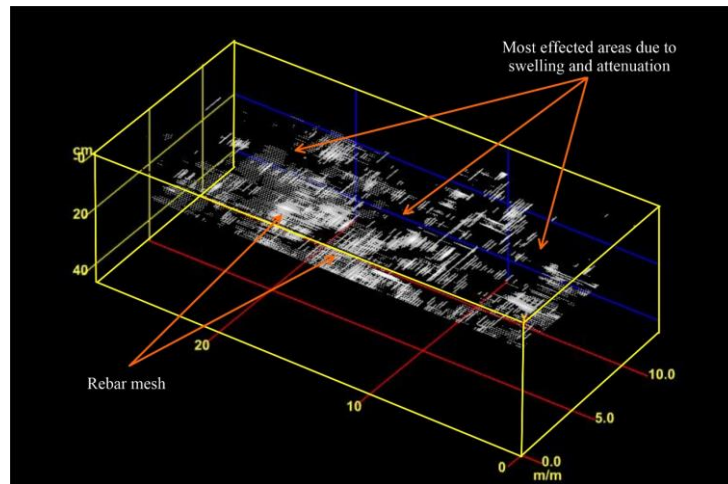


Figure 9. Iso-surface map. Two main areas are present, the rebar mesh area and the area with no reflections

Based on the above results, the GPR method successfully addressed the effect of the pyrite reaction with moisture and other surrounding materials on the concrete slab. This reaction is shown on the GPR profiles as air-void reflections, pushed-up reflections, and dropped-down reflections. Further, the pyrite reaction also appeared as an attenuation that affects the GPR waves to produce very weak reflections. These results provide valuable information about the condition of the concrete slab and the underlying materials, which highlights the extent of deformation in the concrete slab due to the influence of the pyrite swelling effect.

4. Conclusion

Pyrite swelling in concrete slabs is a major issue. Many cases have been registered in Quebec since the 1960s. The use of the GPR method to trace pyrite swelling in concrete slabs is investigated in this paper. In order to detect pyrite swelling in slabs on grade, an extensive assessment is applied using the GPR method in a selected site that occurs in the city of Laval, Quebec. Before the GPR survey, soil samples were collected to determine the soil composition behind the concrete slab. The analysis revealed the presence of limestone, which is more clayey in places and probably intersects thin clayey beds, severe and shale sediments. These sediments are known to have a higher tendency to produce pyrite swelling. The GPR investigation identified three types of reflections: rebar, air-void, and utility reflections. The most important reflections that indicate the pyrite swelling are the rebar reflections. These reflections show a clear deformation in their shapes and places, indicating that the concrete slab is exposed to severe distortion due to pyrite swelling. This deformation is presented on the GPR profiles in the form of pushed-up and dropped-down reflections. The effect of the pyrite swelling on GPR reflections can be recognized in two means. Firstly, the attenuated reflections that may occur as a result of pyrite-rich materials. Secondly, the high-amplitude reflections that may occur due to the presence of air voids. These air voids can be caused due to pushing the concrete slab as a result of pyrite swelling. The 3D Iso-surface map provided valuable information about the most affected areas of the concrete slab. The deformed locations can be recognized easily compared with intact locations. In conclusion, the results indicate that GPR is an effective and reliable method for assessing and mapping the deformations in concrete slabs. It has the capability to locate areas of deformation without the need for extensive excavation work. This makes GPR a valuable tool for addressing the pyrite swelling issues in concrete slabs and ensuring the structural integrity of buildings.

5. Declarations

5.1. Author Contributions

Conceptualization, N.K.A. and G.J.A.; methodology, N.K.A. and G.J.A.; formal analysis, N.K.A.; writing—original draft preparation, N.K.A. and G.J.A.; writing—review and editing, N.K.A. and G.J.A. All authors have read and agreed to the published version of the manuscript.

5.2. Data Availability Statement

The data presented in this study are available on request from the corresponding author.

5.3. Funding and Acknowledgements

This research was supported by the Mitacs Acceleration Program in partnership with Groupe ABS. The authors gratefully acknowledge the financial support provided through this program, which facilitated the execution of the research activities described in this paper.

5.4. Conflicts of Interest

The authors declare no conflict of interest.

6. References

- [1] Anderson, W. H. (2008). Foundation problems and pyrite oxidation in the Chattanooga Shale, University of Kentucky, Estill County, Kentucky. Report of Investigations--KGS. University of Kentucky, Lexington, United States. doi:10.13023/kgs.ri18.12.
- [2] Maher, M., & Gray, C. (2014). Aggregates prone to causing pyrite-induced heave: How they can be avoided. Proceedings of the 17th Extractive Industry Geology Conference, September 2014, Ormskirk, United Kingdom.
- [3] ACQC. 1999. Pyrite and Your House. Association des Consommateurs pour la Qualité Dans la Construction, Montréal, Canada. (In French).
- [4] Nixon, P. J. (1978). Floor heave in buildings due to the use of pyritic shales as fill material. *Chemistry and Industry*, March, 160-164.
- [5] Yamanaka, T., Miyasaka, H., Aso, I., Tanigawa, M., Shoji, K., & Yohta, H. (2002). Involvement of sulfur- and iron-transforming bacteria in heaving of house foundations. *Geomicrobiology Journal*, 19(5), 519–528. doi:10.1080/01490450290098487.
- [6] Hawkins, A. B. (2014). Implications of pyrite oxidation for engineering works. In *Implications of Pyrite Oxidation for Engineering Works*. Springer International Publishing, Cham, Switzerland, doi:10.1007/978-3-319-00221-7.
- [7] Cripps, J. C., Reid, J. M., Czerewko, M. A., & Longworth, I. (2019). Tackling problems in civil engineering caused by the presence of pyrite. *Quarterly Journal of Engineering Geology and Hydrogeology*, 52(4), 481–500. doi:10.1144/qjgeh2019-024.
- [8] Hoover, S. E., Wang, M. C., & Dempsey, B. (2004). Structural damage induced by pyritic shale. *International Conference on Case Histories in Geotechnical Engineering*, 13-17 April, 2004, Missouri, United states.
- [9] Maher, M. L. J., Azzie, B., Gray, C., & Hunt, J. (2011). A large scale laboratory swell test to establish the susceptibility to expansion of crushed rock containing pyrite. Proceedings of the 14th Pan-Am CGS Geotechnical Conference, 1-7 October, 2011, Toronto, Canada.
- [10] McKeon, É. P., O'Connell, A. M., & McCabe, B. A. (2017). Laboratory foundation model with pyrite-bearing mudstone fill. *International Journal of Physical Modelling in Geotechnics*, 17(4), 204–219. doi:10.1680/jphmg.16.00001.
- [11] Conyers, L. B. (2004). *Ground-penetrating Radar for Archaeology*. AltaMira Press, California, United States.
- [12] AL-Hameedawi, M. M., Thabit, J. M., & AL-Menshed, F. H. (2023). Electrical resistivity tomography and ground-penetrating radar methods to detect archaeological walls of Babylonian houses near Ishtar temple, ancient Babylon city, Iraq. *Geophysical Prospecting*, 71(9), 1792–1806. doi:10.1111/1365-2478.13293.
- [13] Pajewski, L., Benedetto, A., Derobert, X., Giannopoulos, A., Loizos, A., Manacorda, G., Marciniak, M., Plati, C., Schettini, G., & Trinks, I. (2013). Applications of Ground Penetrating Radar in civil engineering - COST action TU1208. 2013 7th International Workshop on Advanced Ground Penetrating Radar. doi:10.1109/iwagpr.2013.6601528
- [14] Knight, R. (2001). Ground penetrating radar for environmental applications. *Annual Review of Earth and Planetary Sciences*, 29(1), 229–255. doi:10.1146/annurev.earth.29.1.229.
- [15] Busby, J., Cuss, R., Raines, M., & Beamish, D. (2004). Application of ground penetrating radar geological investigations. *British Geological Survey*, Keyworth, United Kingdom.
- [16] Mellett, J. S. (1995). Ground penetrating radar applications in engineering, environmental management, and geology. *Journal of Applied Geophysics*, 33(1–3), 157–166. doi:10.1016/0926-9851(95)90038-1.
- [17] Balkaya, Ç., Kalyoncuoğlu, Ü. Y., Özhanlı, M., Merter, G., Çakmak, O., & Talih Güven. (2018). Ground-penetrating radar and electrical resistivity tomography studies in the biblical Pisidian Antioch city, southwest Anatolia. *Archaeological Prospection*, 25(4), 285–300. doi:10.1002/arp.1708.
- [18] Neal, A. (2004). Ground-penetrating radar and its use in sedimentology: Principles, problems and progress. *Earth-Science Reviews*, 66(3–4), 261–330. doi:10.1016/j.earscirev.2004.01.004.
- [19] Oikonomopoulou, E. C., Palieraki, V. A., Sfikas, I. P., & Trezos, C. G. (2022). Reliability and limitations of GPR for identifying objects embedded in concrete – Experience from the lab. *Case Studies in Construction Materials*, 16, 898. doi:10.1016/j.cscm.2022.e00898.

- [20] Liu, H., Lin, C., Cui, J., Fan, L., Xie, X., & Spencer, B. F. (2020). Detection and localization of rebar in concrete by deep learning using ground penetrating radar. *Automation in Construction*, 118, 103279. doi:10.1016/j.autcon.2020.103279.
- [21] Tian, H., Zhou, Z., Zhang, Y., & Wei, Y. (2020). Axial behavior of reinforced concrete column with ultra-high performance concrete stay-in-place formwork. *Engineering Structures*, 210, 110403. doi:10.1016/j.engstruct.2020.110403.
- [22] Pérez-Gracia, V., González-Drigo, R., & Di Capua, D. (2008). Horizontal resolution in a non-destructive shallow GPR survey: An experimental evaluation. *NDT and E International*, 41(8), 611–620. doi:10.1016/j.ndteint.2008.06.002.
- [23] Abdul Rahman, M., Donda, D., Latosh, F., Tarussov, A., & Bagchi, A. (2022). Entropy evaluation of subsurface materials and defects in Concrete Slabs using GPR. 11th International Conference on Structural Health Monitoring of Intelligent Infrastructure, 8-12 August, 2022, Montreal, Canada.
- [24] Dinh, K., & Gucunski, N. (2021). Factors affecting the detectability of concrete delamination in GPR images. *Construction and Building Materials*, 274, 121837. doi:10.1016/j.conbuildmat.2020.121837.
- [25] Rasol, M. A., Pérez-Gracia, V., Fernandes, F. M., Pais, J. C., Santos-Assunção, S., Santos, C., & Sossa, V. (2020). GPR laboratory tests and numerical models to characterize cracks in cement concrete specimens, exemplifying damage in rigid pavement. *Measurement*, 158, 107662. doi:10.1016/j.measurement.2020.107662.
- [26] GSSI Handbook. (2003). Geophysical Survey Systems, Inc., North Salem, United States. Available online: www.geophysical.com (accessed on February 2024).
- [27] Procedure CTQ-M200. (2001). Appraisal procedure for existing residential buildings. Quebec Technical Committee for the Study of Swelling, Quebec City, Canada.